Micromechanics and Damage in Slide-Ring Networks

Samuel C. Lamont, Kyle Weishaar, Carson Bruns, and Franck J. Vernerey*

University of Colorado at Boulder, Boulder, Colorado, 80309, USA

(Dated: January 2, 2024)

We explore the mechanics and damage of slide-ring gels by developing a discrete model for the mechanics of chain-ring polymer systems that accounts for both crosslink motion and internal chain sliding. The proposed framework utilizes an extendable Langevin chain model to describe the constitutive behavior of polymer chains undergoing large deformation and includes a rupture criterion to innately capture damage. Similarly, crosslinked rings are described as large molecules that also store enthalpic energy during deformation and thus have their own rupture criterion. Using this formalism, we show that the realized mode of damage in a slide-ring unit is a function of the loading rate, distribution of segments, and inclusion ratio (number of rings per chain). After analyzing an ensemble of representative units under different loading conditions, we find that failure is driven by damage to crosslinked rings at slow loading rates, but polymer chain scission at fast loading rates. Our results indicate that increasing the strength of the crosslinked rings may improve the toughness of the material.

I. INTRODUCTION

In recent years, hydrogels have been of particular interest to the field of polymer science as many of their designs exhibit biocompatibility [1], controllable stiffness [2], and the ability to self-heal [3]. This makes them desirable for many applications ranging from tissue engineering [4] to adhesives [5]. However, many potential applications of conventional gels are limited by their fragile nature. In order to overcome this key limitation, a variety of novel gels have been proposed [6]. These gels use specialized network structures to improve their mechanical strength and include double-network gels [7, 8], nanocomposite gels [9, 10], and slide-ring gels [5, 11]. Slide-ring gels are comprised of polymer chains threaded by ring-like molecules that are crosslinked together to form sliding junction points. Such gels exhibit many exceptional properties such as the ability to recover from extreme deformations [12], a low elastic modulus [13], and a high fracture toughness [14]. Despite these remarkable features, slide-ring gels have a low mechanical strength that must be improved before they can be used for structural applications [15].

A conventional chemical gel is composed of polymer chains that are crosslinked with strong bonds at various junctions, thereby forming a network of subchains that meet at crosslinking junctions. Due to the crosslinking process as well as natural polydispersity in chain length after polymerization, there may be a wide variance in subchain length distribution [16]. This inhomogeneity in chain length is largely cited as the driving factor for a conventional gel's fragility, as stress is thought to become concentrated on shorter segments [17, 18]. In turn, this leads to localization and void nucleation, which begins the brittle fracture process [19]. By contrast, the architecture of slide-ring gels offers an intrinsic mechanism for

avoiding these inhomogeneities and their resulting vulnerability to localization. In these systems, the crosslinking junctions are replaced by ring-like molecules through which the underlying polymer network may freely slide [20]. This allows the polymer chains to equalize the tension held in its various sub-sections, thus increasing the stress a network may sustain before rupturing. As a result, it is believed that the mechanical strength of a slidering gel is not limited by network inhomogeneities, but rather the strength of the weakest network component [13, 21]. While the distribution of forces in a slide-ring network are more uniform, it is still not trivial to determine the network component (chains, crosslinkers, etc.) that is the most vulnerable to breaking. This is not only a function of the dissociative bond energies of the network components, but also network topology as well as loading conditions. Damage initiation in these gels must therefore be studied at the level of a network, rather than that of a single chain.

Many classical constitutive models estimate the behavior of a polymer network by considering the mechanical response of a representative unit cell. For instance, the classical 3-chain model considers a unit cell composed of three chains that are each aligned with the loading's principal directions [22]. Such models typically assume that chains follow an affine deformation, where the motion of a single chain is governed exactly by the macroscopic deformation. Furthermore, the length of a chain is considered to be uniform and unchanging. In contrast, the chains forming a slide-ring network are constantly changing their length, which is expected to result in largely non-affine motion. A model by Ito [20] aimed at reconciling this particular shortcoming by allowing for the redistribution of chain segments within a 3-chain formulation. While this was found to explain some of the behavior of slide-ring systems, it was not until five years later that a key missing ingredient was added in the form of a novel ring entropy thought to arise from the rings that remained uncrosslinked after the gelation process [23]. These so-called "mobile" rings

^{*} correspondence to: franck.vernerey@colorado.edu

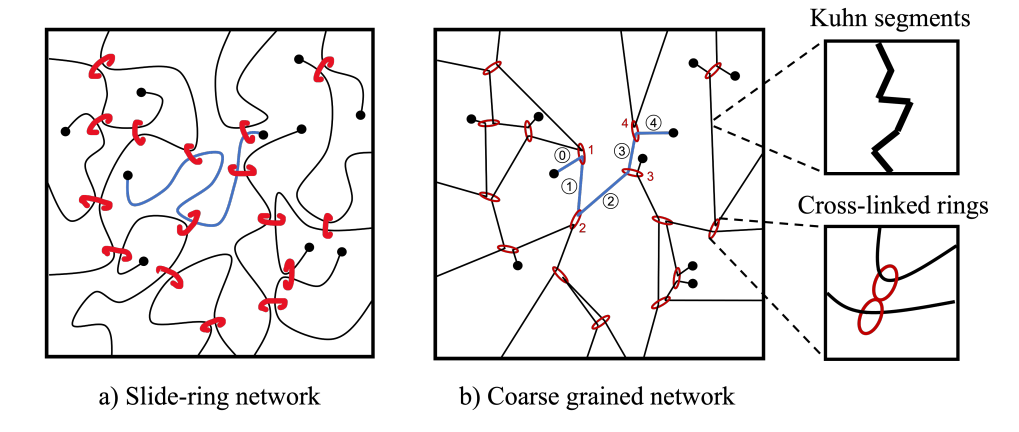


FIG. 1: Slide-ring network and its components. a) Depiction of a slide-ring network with chains (black lines), rings (red), and stoppers (black dots). b) The coarse grained model separates each chain into a collection of crosslinked rings and subchains. Crosslinked rings on a chain are numbered from left to right starting from 1 to N. Similarly, subchains are numbered from 0 to N starting from a dangling end.

are currently thought to source an osmotic force that ultimately drives, or hinders, the motion of chains within the network [24, 25]. Recently, this idea was formalized in a continuum model using the Transient Network Theory [26], which could explain key features of the viscoelastic response of slide-ring gels. This formalism has also been used to investigate damage in shear thinning polymers [27] and dynamic polymer networks [28].

While continuum models have been able to capture many of the complex behaviors of slide-ring systems, they are ill-suited to study network-level dynamics. On the other hand, molecular dynamics simulations have provided valuable insights into the smaller-scale physics that govern the system. For example, coarse grained simulations have been employed to show that chain sliding reduces tension in a network [29], to link chain sliding to a network's elastic response [30], and to explore the damage mechanisms within a slide-ring gel [31]. However, molecular dynamics are often computationally expensive and are unable to model the long-term behavior of large slide-ring networks. Alternatively, mesoscale (or network) models consider a more heavily coarse-grained system and have a relatively low computational cost. A variety of network-level physics may be investigated within this framework; for instance, dynamic crosslinking events in star-shaped polymers [32, 33] as well as topological rearrangement due to reptation and chain sliding [34]. The advantage of studying systems at this lengthscale is a compromise between incorporating small-scale physics and computational simplicity

In this study, we extend the concept of a single chain model to study the mechanical behavior of a slide-ring unit (a single chain) connected to the surrounding network via sliding connections (or rings). This unit is assumed to interact with an effective medium, where crosslinking points (but not the chains) deform affinely. To describe the mechanical response of the unit, together

with the development of internal forces within its elements (subchains and rings), we develop a thermodynamically consistent model that accounts for the combined entropic and enthalpic contributions of flexible chains and mobile rings and their limit stretch. This enables us to investigate the force-response and damage initiation in the slide-ring unit as a function of its orientation in the network and macroscopic loading conditions. We identify various damage mechanisms, which depend on loading rates and the relative strengths of the chains and the rings.

II. PHYSICAL LAWS OF A SLIDE-RING SYSTEM

We begin by deriving the basic physical laws that govern a slide-ring system. Slide-ring gels are comprised of flexible polymer chains threaded by ring-like molecules (Fig. 1a) and stopped by a bulky end-group. Historically, the backbone molecule is polyethylene glycol (PEG) and the rings are α -cyclodextrin (CD) molecules, but other systems have been synthesized [35, 36]. For this study, we consider the most common PEG-CD system. Furthermore, we assume that each ring can freely move along its respective chain up to the stopper. To form a network, two rings are crosslinked together, forming a figure-eight structure that connects neighboring chains. After the crosslinking process, there exist a number of uncrosslinked rings (mobile rings) that remain untethered to the network, but are still restricted to slide along their respective chain.

Conceptually, a slide-ring gel can be described as a connected network of subchains and crosslinked rings illustrated in Fig. 1b. With this description, a subchain is denoted as the portion of the polymer chain (including any threaded mobile rings) that is between

two crosslinked rings or a stopper. Thus, a ring-chain unit with N crosslinked rings is comprised of N+1 subchains. Furthermore, the $i^{\rm th}$ subchain of the unit may be discretized into a collection of n_i freely joint Kuhn segments of length b_i , such that its contour length is $n_i b_i$. We also define the end-to-end vector \mathbf{r}_i , which spans the distance between the two crosslinked rings adjacent to the $i^{\rm th}$ subchain. Subchains i=0 and i=N are referred to as dangling ends as they are capped by a stopper; while they may contain a reserve of Kuhn segments, their end-to-end vector is not constrained in space and is thus treated as zero.

A. Motion and damage

We now discuss the physical processes that occur when the system is perturbed from equilibrium. As discussed previously, every subchain is threaded by mobile rings that are assumed to be in constant motion due to thermal fluctuations. As a result, the i^{th} subchain experiences a one-dimensional osmotic force π_i directed along the contour of the chain (Fig. 2a) [26]. Differences in this osmotic force drive chain sliding between subchains as Kuhn segments move from subchains with a high osmotic force to subchains with a low osmotic force. This process is not instantaneous, but rather a time-dependent process that is subject to frictional forces between the polymer chain and the crosslinked rings. Let $\dot{\vartheta}_i$ represent the velocity of a chain sliding through its ith crosslinked ring and ζ be a time-dependent frictional parameter. This relationship can be represented as

$$\zeta \dot{\vartheta}_i = [\pi]_i, \tag{1}$$

where $[\pi]_i = \pi_{i+1} - \pi_i$ is the osmotic force differential across the i^{th} ring. The total change in segment number within a subchain depends on the chain's velocity at both adjacent crosslinked rings. Thus, the number of segments in the i^{th} subchain is changing at a rate of $\dot{n}_i = \dot{\vartheta}_{i+1} - \dot{\vartheta}_i$.

Next, we turn to the absolute motion of a crosslinking junction. For this, we first note that a figure-eight junction may be described as two individual rings that are connected via a covalent junction. For simplicity, we assume here that the bond only carries tensile forces such that each ring within the i^{th} figure-eight applies an equal and opposite force f_i onto one-another. Besides, a ring is also subjected to the forces from a threaded chains, that takes the form of the vector $[t]_i = t_{i+1} - t_i$. Now considering that a ring (at current position x) is immersed in a solvent characterized by viscosity μ , its velocity is determined by the over-damped equation:

$$\mu \dot{\boldsymbol{x}}_i = \boldsymbol{f}_i - [\boldsymbol{t}]_i. \tag{2}$$

This equation of motion is schematically represented in Fig. 2b. Finally, we discuss the concept of damage as occurring at the extreme limits of these processes. The formalism used here is similar to the extendable chain

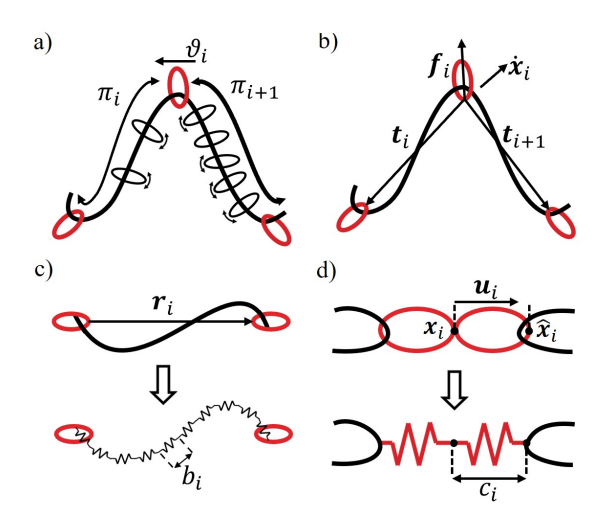


FIG. 2: Motion and damage in a slide-ring system. a) Chain sliding is driven by an osmotic force differential $[\pi]_i$ between subchains, whose source is mobile rings threaded along the chain. b) Translational motion of a crosslink is driven by a force differential between adjacent subchains, $[t]_i = t_{i+1} - t_i$ and the force exerted by the adjoined ring, f_i . c) Kuhn segments are modeled as springs with resting length b'. Each Kuhn segment in a subchain i is assumed have the same length b_i . d) crosslinked rings are modeled as two springs of length c_i in series. The crosslinked rings are joined at the point x_i and the chain is attached on the opposite side of the ring \hat{x}_i .

model presented by Mao et al. [19] and its expansion to crosslinking junctions [37]. In brief, we model the components of each subchain as storing their own elastic energy. Thus, each crosslinked ring acts as a spring of length c_i and each Kuhn segment acts as a spring of length b_i (Fig. 2c and Fig. 2d). To maintain a simple damage criterion, we assume that these components may break after being stretched past a specified limit. Thus, we track the motion of not only the end-to-end vectors of the polymer chain, but also the stretch of the Kuhn segments and crosslinked rings. For this, we require a framework for describing the positions and orientation of the rings. Let x_i be the position vector of the junction point of a set of crosslinked rings and \hat{x}_i be the position vector of the diametrically opposite position on the ring. We assume that the junction of the polymer chain and the ring exists at \hat{x}_i and define the unit vector $u_i = (\hat{x}_i - \hat{x}_i)$ $|x_i|/|\hat{x}_i-x_i|$ to describe the orientation of the crosslinked ring (Fig. 2d).

B. Free energy of a single chain

The behavior described in the previous question prompts three key questions regarding our system: (i) what is the osmotic pressure that drives relative chain motion, (ii) what is the chain-force that drives crosslink motion, and (iii) under what conditions do Kuhn segments or crosslinked rings fail. To answer these questions, we here follow the general approach described in [38] to develop a Helmholtz free energy functional for a single slide-ring chain. The free energy is constructed by considering entropic constributions, which scale with temperature T, and enthalpic contributions, which are purely elastic. In a polyrotaxane chain, contributions from both the polymer chain and the ring molecules are present. For the remainder of the manuscript, we reserve a sugrescript m for quantities relating to the mobile rings along the chain and a superscript x for quantities relating to the crosslinked rings. Then, our model accounts for the entropic contribution S_i of each subchain's polymer chain, the enthalpic contribution U_i of each subchain's Kuhn segments, the enthalpic contribution U_i^x of each set of crosslinked rings, and the entropic contribution S_i^m of the mobile rings within each subchain. The free energy functional thus takes the general form

$$\mathscr{F} = \sum_{0 \le i \le N} \left[(U_i - TS_i) - TS_i^m \right] + \sum_{1 \le i \le N} U_i^x. \tag{3}$$

Recall, N is the number of crosslinked rings on a chain and subchains are numbered from 0 to N. Hence, the first summation is performed over subchains while the second summation is performed over crosslinked rings. The following paragraphs define the explicit form of each term in this equation. For brevity, we omit the subscript i in the following derivations.

Beginning with the entropic energy of mobile rings threaded on the chain, we follow the definitions presented in our previous work [26], which are similar in form to the original mobile ring entropy proposed by Mayumi et al. [23]. We consider a subchain is composed of n Kuhn segments threaded by p mobile rings. By definition, the entropy generated by the mobile rings is of the form $S^m = k_b \log(\Omega)$ where Ω is the total number of possible ring configurations on the subchain. Assuming that each mobile ring occupies one Kuhn segment and each Kuhn segment has an equal probability of being occupied, this takes the form of the binomial $\binom{n}{p}$. After taking the logarithm and simplifying the following expression using Stirling's approximation [39], we obtain the required expression:

$$S^{m} \approx k_{b}(n\log(n) - (n-p)\log(n-p)). \tag{4}$$

Note that we have neglected all timescales and energy dissipation arriving from mobile ring diffusion. This assumes that mobile rings remain in equilibrium and are able to move along the chain at a timescale much faster than the relaxation time of the unit. As we are eventually interested in the initiation of damage in a slide-ring system, we require a description of chain entropy that is valid for extensions up to the contour length of the chain. The most commonly used formulation was proposed by Kuhn and is referred to as the Langevin model [40]. In

our system, note that the contour length of a chain may change due to varying the number of Kuhn segments n or their length b. Furthermore, the Langevin function may be explicitly approximated by the Padé approximation proposed by Cohen [41], $\mathcal{L}^{-1}(x) \approx x(3-x^2)/(1-x^2)$, which is valid for the required domain of $0 \le x \le 1$. The resulting chain entropy functional takes the form:

$$S \approx -nk_b \left[\frac{1}{2} \left(\frac{r}{nb} \right)^2 - \ln \left(1 - \left(\frac{r}{nb} \right)^2 \right) \right].$$
 (5)

Moving on to enthalpic considerations, when a subchain's end-to-end vector approaches its contour length, the Kuhn segments may be physically strained before reaching their rupture point [42]. To capture this enthalpic stretch, we extend the Langevin model following the approach presented in [19], which treats Kuhn segments as elastic springs that may store their own enthalpic energy. The simplest form of this enthalpic energy is a harmonic potential, which approximates each segment as a linear spring. Assuming that each Kuhn segment in one subchain is stretched equally, the enthalpic contribution of all n Kuhn segments in a subchain is the product

$$U = n\frac{E}{2} \left(\frac{b}{b'} - 1\right)^2,\tag{6}$$

where E, with units of energy, is the elastic stiffness of bonds in the chain's backbone and b' is the resting length of a Kuhn segment [19].

Finally, we consider the enthalpic energy of crosslinked rings. The movement of these rings is constrained by the tension in its adjacent subchains. If the tension in the surrounding subchains is sufficiently large, crosslinked rings may begin to stretch and eventually rupture. To account for this, we model a set of crosslinked rings as two springs in series with stiffness E^x and resting length c' [37]. Once again, we use a harmonic potential as a simple energetic penalty for stretching the rings. The enthalpic contribution of a crosslinked ring thus becomes

$$U^x = \frac{E^x}{2} \left(\frac{c}{c'} - 1\right)^2,\tag{7}$$

C. Driving thermodynamic quantities

We may now answer the questions introduced in the previous section using the formalised free energy of Eq. (3). Notice that each subchain has three quantities that may vary to minimize its free energy: the end-to-end vector \mathbf{r} with length r, the number n of Kuhn segments, and the length b of each Kuhn segment. Furthermore, the length c of each crosslinked ring must be treated as their own independently varying quantities. Each of these quantities will evolve to minimize the free energy of the full chain, which ultimately gives rise to the forces that drive the motion outlined in section II A. Beginning

with the osmotic force π , we take the derivative of the free energy with respect to n to yield

$$\pi = \Lambda(r, n, b) - \frac{k_b T r^2}{b^2 n^2} \left(\frac{r^2 - 3n^2 b^2}{r^2 - n^2 b^2} \right) + k_b T \log(1 - \frac{p}{n})$$
(8)

where the factor Λ is:

$$\Lambda = \frac{E}{2} \left(\frac{b}{b'} - 1 \right)^2 + k_b T \left[\frac{1}{2} \left(\frac{r}{nb} \right)^2 - \log \left(1 - \left(\frac{r}{nb} \right)^2 \right) \right]. \tag{9}$$

It is worth noting that as r approaches 0, Eq. (3) converges to the energy functional based on Gaussian chain physics (provided n is sufficiently large). Next, we take the derivative with respect to r to yield the tension \mathbf{t} held in a flexible subchain,

$$t = \frac{k_b T}{nb^2} \left(\frac{r^2 - 3n^2 b^2}{r^2 - n^2 b^2} \right) r, \tag{10}$$

where b is determined by minimizing the free energy, i.e. finding b such that $\mathscr{F}_{,b}=0$ [28]. Note that we consider b to remain in equilibrium, i.e., that the timescale associated with stretching the Kuhn segment is very fast. As defined in Eq. (2), the opposing force of this tension is provided by the crosslinked rings. As the only term involving c is the enthalpic energy U, we may take the derivative directly to yield

$$f = \frac{E^x}{c'} \left(\frac{c}{c'} - 1\right) u,\tag{11}$$

where c is determined by minimizing the free energy with respect to c. To consider a damage criterion for our system, we follow the approach of Mao et al. [19, 37] and postulate that a component (here, either a Kuhn segment or a crosslinked ring) fails once a critical rupture energy is exceeded (i.e. in Eq. (6) or Eq. (7)). Physically, this corresponds to the bond storing more energy than required for dissociation. In practice, this requires determining the current Kuhn segment length b or ring length c and determining if a critical stretch has been exceeded. Once the critical energy has been exceeded, the component is considered to rupture [19]. This is discussed further in the following section.

III. TRANSIENT MECHANICS OF AN ALIGNED CHAIN

To gain insight into the transient mechanics of a slidering system, we here consider the response of a single slide-ring chain composed of two crosslinked rings (Fig. 1a). Such a chain contains only one internal subchain, ensuring both crosslinked rings are adjacent to a tension-free dangling end. We refer to this system as an aligned chain as all forces are aligned in the direction of the end-to-end vector \mathbf{r} . For this study, we assume that each subchain is initially composed of n = 50 Kuhn segments,

yielding $n_t = 3n = 150$ total segments in the full chain. Additionally, we assign p = 10 mobile rings to thread each subchain. The stiffness of both a Kuhn segment and crosslinked ring is taken to be that of a carbon to carbon bond, the weakest bond in the polyethylene glycol chain, which was previously estimated to be $E_{C-C} = 2300k_bT$ [19]. For the remainder of this manuscript, we present bond stiffnesses in units of E_{C-C} , thus, E = 2 means $E = 2E_{C-C} = 4600k_bT$. Finally, we take the length of a Kuhn segment to be twice the length of a dimer of the backbone polyethylene glycol chain, yielding b' = 22 Angstroms [43].

To set a reference point for the chain-level quantities, we consider the equilibrium state of the chain when the end-to-end vector is r=0. In this condition, there is no tension in the subchains and the Kuhn segments are evenly distributed throughout the chain. Thus, each subchain has $n'=n_t/(N+1)$ segments and a residual osmotic force of $\pi'=-k_bT\log(1-\frac{p}{n'})$. Furthermore, the minimum number of segments in a chain is equal to the number of mobile rings, thus, the maximum number of segments in the center of the chain is $n_{\infty}=n_t-2p$. As the time-dependent behavior of the chain is governed by the timescale of sliding, we define the following non-dimensional loading parameter:

$$W = \frac{\dot{\lambda}\zeta}{k_b T},\tag{12}$$

where λ is the rate at which the endpoints are separated. This parameter thus governs the competition between sliding, which tends to dissipate energy, and stretching, which stores elastic energy. When W is low, chain sliding occurs at a much faster timescale than the loading rate and energy is dissipated immediately. Alternatively, the chain behaves elastically for large values of W. Fig. 3 plots the chain tension t, number of segments in the middle subchain n, and Kuhn segment and ring stretch b'/b and c'/c, respectively, for different values of W. Note that the tension is plotted on a logarithmic axis to better visualize the response at high stretches and all quantities have been normalized by their reference values. In particular, we normalize n such that it vanishes at equilibrium (n = n') and approaches 1 after the dangling ends have been depleted $(n = n_{\infty})$. We begin the analysis by discussing the limiting cases of fast and slow loading $(W \to \infty \text{ and } W \to 0, \text{ respectively}).$

A. Rate-dependent chain response

Fast loading. A chain that is deformed at a sufficiently fast rate does not have time to slide through its crosslinked rings. In this case, the effects of chain sliding are negligible and the crosslinked rings can be treated as permanent bonds. As a result, the governing equations (Eqs. (1) and (2)) become $\mathbf{f} = [\mathbf{t}]$ and $\dot{\vartheta} = 0$, which dictates that n remains constant. This regime is illustrated

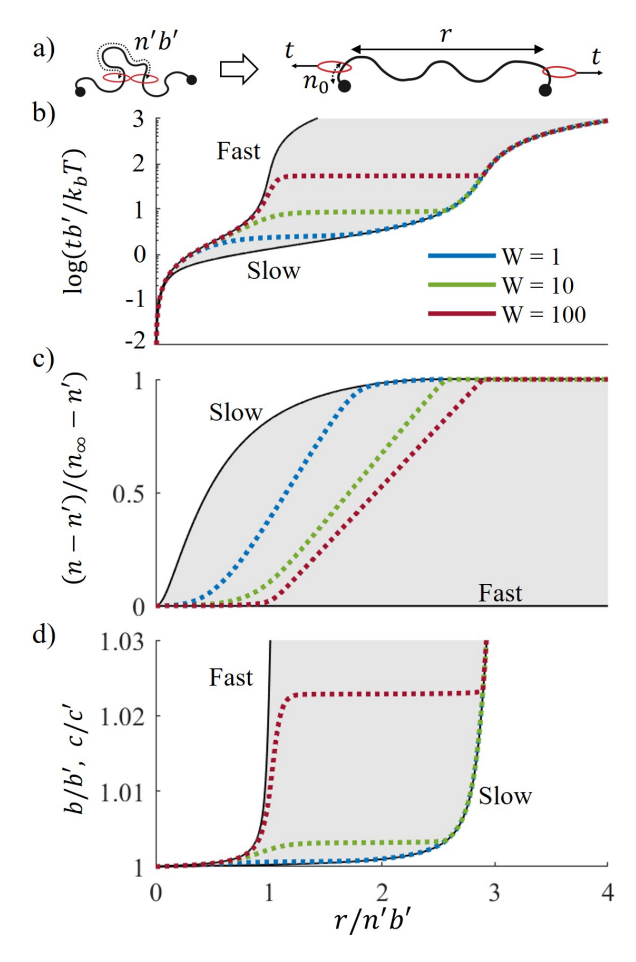


FIG. 3: The mechanical response of a single chain being separated at different rates. The limiting regimes of fast and slow loading are illustrated with fine black lines, while intermediate loading rates are shown as colored dashed lines. Note that all quantities have been normalized by their reference quantities.

by the black lines in Fig. 3b-d labeled "fast." Note the two force regimes characteristic of this scenario (Fig. 3b), separated by the point at which chain components begin to stretch (Fig. 3d), which occurs close to the contour length of the reference chain (i.e., $r \approx n'b'$). Before this point, the tensile force of the internal subchain follows the Langevin chain model for a chain with contour length b'n'. However, as the chain is stretched further, it stiffens to the point that the Kuhn segments and crosslinked rings start to stretch. As a result, the tension does not diverge with further increase in r. Note that this follows the behavior of the extendable chain model proposed by Mao et al. [19]. Clearly, sliding is not possible in this regime, which ensures that n = n' for all r (Fig. 3c).

Slow loading. The slow loading limiting case is obtained when the rate of deformation is much less than the rate of chain sliding. Thus, the chain is permanently in a stable configuration, with no differential of osmotic force across the chain. The governing equations for the

slow loading response are f = [t] and $[\pi] = 0$. The solutions to these equations are illustrated by the black lines in Fig. 3b-d labeled "slow." For this case, there are three regimes of response during the loading history. When loading begins, the segments in the dangling end move into the internal subchain due to the increase in osmotic force (Fig. 3c). The chain tension thus softens as the contour length of the middle subchain grows. However, there is a limited number of Kuhn segments in the dangling ends. Indeed, as n approaches its maximum value of n_{∞} (implying that all Kuhn segments have moved into the middle subchain), the force response of the internal subchains briefly converges to the Langevin model for a chain with n_{∞} segments. Similar to the fast loading case, the point at which segment and ring stretch becomes significant may be defined as another transition point. Note that this occurs around the point $r \approx 3n'b'$ because there are three total subchains (Fig. 3d). Consequently, when the chain is stretched past this point, the force response of the inner subchain diverges from the corresponding Langevin model in a similar manner as before.

Intermediate loading rates. Finally, we may discuss the behavior of the chain at intermediate loading rates. In this scenario, there exists a competition between storing elastic energy by stretching and dissipating energy by sliding. In Fig. 3b-d, we illustrate the response of three loading rates defined by W = 1, W = 10, and W = 100. Notice that all three of these curves lie within the boundaries of our fast and slow limiting cases discussed previously. For these loading rates, we again notice three distinct regimes. Similar to the slow and fast loading cases, the initial tensile response is dictated by the elastic behavior of a chain with contour length n'b' (Fig. 3b). Eventually, a regime of sliding occurs, which represents a smooth transition from the elastic response to the equilibrium response. The boundaries of this regime are indicated by n > n' and $n \to n_{\infty}$ (reflected by the transition from 0 to 1 in Fig. 3c). Notice that the width of these boundaries indicates the rate at which energy is dissipated with respect to the increase of r. This is also reflected in the force response, which becomes more horizontal as the dissipation rate increases, indicating that the applied energy is primarily being used to drive sliding. Furthermore, we note that all three quantities (force, segment count, and component stretch) transition from the fast response to the slow response during the sliding regime. Once the dangling ends have been depleted, sliding halts and all curves converge back to the slow loading case.

B. Damage behavior

The damage behavior of the aligned chain is governed by the relative loading rate W and the strength of the weakest component. As discussed previously, the damage criterion considered in this study is ultimately based on a critical bond dissociation energy; when the enthalpic

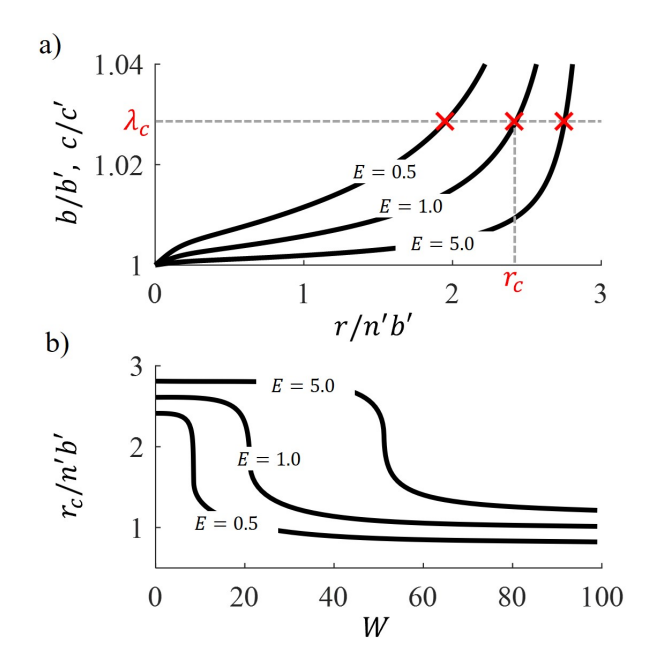


FIG. 4: Damage behavior of the aligned chain in the slow loading regime $(W \to 0)$ with $E^x = E$. a) Component stretch versus normalized end-to-end distance for different component stiffnesses. At a critical stretch λ_c , the component is assumed to fail. b) Critical separation distance $r_c/n'b'$ versus normalized loading rate for different component stiffnesses.

energy of a component (rings or Kuhn segments) has exceed this critical energy, it breaks. With the harmonic potentials defined in Eqs. (6) and (7), this may also be considered as a critical stretch λ_c after which the respective component has stored its critical energy. As a result, two parameters directly govern component-wise failure: the stiffness E^K or E^R and the critical stretch λ_c , which may be varied for rings or Kuhn segments as well.

Let us consider the damage behavior of the aligned chain with varying stiffnesses but a constant critical stretch (Fig. 4). If the stiffness of a component, E^x or E for crosslinked rings or Kuhn segments, respectively, is less than E_{C-C} , the component begins stretching at an earlier separation distance. Thus, the component reaches its critical stretch λ_c at a smaller critical separation distance r_c . Alternatively, increasing the stiffness of the component results in higher resistance to stretching and, thus, a larger critical separation distance. Let us first use $E^x = E$ to illustrate the trends of our model. In this case, the stretch b/b' of the Kuhn segments and the stretch c/c' of the rings is always the same – if one component were weaker, failure would always be dictated by that component.

Fig. 4a plots the component stretch b/b' (or, alternatively, c/c') versus the normalized separation distance r/n'b' for three values of component stiffness: (i) E=5, (ii) E=1, and (iii) E=0.5 for the case of slow loading, i.e. $W\to 0$. The dashed grey lines indicate the

critical stretch and corresponding critical separation distance (only illustrated on the E=1 curve for brevity) for the three cases. For E=0.5, the components begin to stretch almost immediately with an increase in r. This regime thus reflects a scenario where the enthalpic stiffness of the Kuhn segments is close to the entropic stiffness of the polymer chain. Here, the critical stretch is reached before the chain has stiffened significantly, which is unlikely for a physical polymer chain. In contrast, strengthening the components by a factor of five delays component stretch as the entropic stiffness of the chain is much softer than the enthalpic stiffness of the components. Thus, the polymer chain is well into its stiffening regime before the components stretch significantly.

To demonstrate the dependence of damage with respect to relative loading rate, we plot in Fig. 4b the normalized critical separation distance $r_c/n'b'$ versus loading rate for the same range of component stiffnesses. Generally, with larger E, we observe a larger critical stretch r_c . Furthermore, we notice a transitional regime between $r_c \approx 3n'b'$ (the contour length of the full chain as there are 3 subchains) and $r_c \approx 1n'b'$ (the initial contour length of one subchain) that occurs at different loading rates. For instance, the critical stretch of E=5 and E=0.5 is similar for W < 10 and W > 50. However, between these loading rates, the chain with E = 5 is able to stretch nearly three times as far as the chain with E = 0.5. Thus, it is important to consider the regime of loading rates that a chain will be subjected to as strengthening its components does not have a large effect at very slow or very fast rates.

IV. DAMAGE MECHANISMS OF A SLIDE-RING UNIT

In an isotropic network, a chain and its subchains may have arbitrary orientation with respect to the loading direction (Fig. 1). We therefore propose a simple study of a well-defined volume element and report on its emergent behavior in terms of damage initiation. The proposed slide-ring unit is a rectangular domain of length L and height H comprised of a chain threaded by N crosslinked rings equispaced along its edges (Fig. 5). The chain connects alternating rings from each side to produce a "zig-zag" pattern. The unit itself may be uniquely defined by its crosslink density $\rho = N/LH$ and the angle created by the exterior subchain and the bottom of the unit $tan(\phi) = (N-1)H/L$, the latter of which may be thought of as a measure of how coiled the chain is in space. For example, $\phi = 0$ describes the perfectly aligned chain described in the previous section. Alternatively, as ϕ approaches $\frac{\pi}{2}$, we observe a perfectly coiled chain that minimizes its occupied volume. Note that this study is performed in 2D to illustrate the basic predictions of the model.

To predict the response of differently oriented units, we consider applying a purely deviatoric deformation in

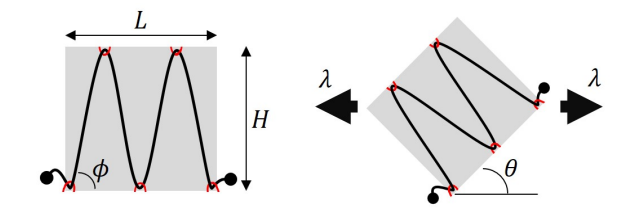


FIG. 5: The simple 2D unit studied in this section is defined by its crosslink density $\rho = N/LH$ and its coil angle ϕ . We consider deviatoric deformations of the unit in an arbitrary direction θ .

an arbitrary direction. For instance, we may consider a global deformation of the form $\mathbf{F} = \mathrm{diag}\{1/\lambda,\lambda\}$, where λ is the macroscopic stretch ratio. While \mathbf{F} is defined in a global coordinate system \mathbf{e}_i , the deformation observed by an arbitrary oriented unit may be considered as the equivalent deformation in its local frame \mathbf{e}_i' . Defining θ as the angle between \mathbf{e}_i and \mathbf{e}_i' , we, therefore, consider a general deformation of the form

$$\mathbf{F'}(\lambda, \theta) = \mathbf{R}(\theta)\mathbf{F}(\lambda)\mathbf{R}(\theta)^{T}, \tag{13}$$

where the orthogonal matrix R defines the orientation of the chain with respect to the principal stretch directions. For convenience, we normalize all lengths in the unit volume by that of an undeformed Kuhn segment b'. To restrict the parameter space, we considered an experimental system of low-inclusion polyrotaxane with low crosslinking density as these systems have been the most highly characterized [44, 45]. According to the experimentally measured crosslinked ring densities on the order of 10 m⁻³ [45], we consider chains with N=5 crosslinked rings, an angle of $\phi=\frac{\pi}{4}$, and a density of $\rho = 0.05 \, b'^{-2}$, where b' is considered as 22 angstroms [43]. As the percentage of crosslinked rings on a single chain was measured to range from 5-36% [45], we choose the number of mobile rings per segment to be p = 8, which corresponds to 10% of the rings being crosslinked on the full chain. Additionally, we assume the full chain contains 100 Kuhn segments, each initially having the reference stiffness of the carbon-carbon bond, $E = E^x = 1$. Furthermore, the critical bond dissociation energy is assumed to be the same for each component, yielding a critical component stretch of $\lambda_c = 1.01$. The number of mobile rings per segment is initially chosen to be p = 8, which reflects a relatively low inclusion polyrotaxane. Finally, we consider the length of a crosslinked ring to be 0.75 times that of a Kuhn segment, which is consistent with the ratio of the outer diameter of an α -cyclodextrin ring (about 15 angstroms [46]) to the length of a polyrotaxane Kuhn segment. These values are summarized in Table I.

Note: The stretch-driven failure criterion implies that stiffening an element (either ring or Kuhn segment) will delay its rupture and therefore make it effectively

stronger. Conversely, a compliant element may be thought of as weak.

Loading parameters	Symbol	Values
Angle of loading	θ	from 0 to 2π
Macroscopic stretch	λ	varied
Network parameters	Symbol	Values
Number of crosslinked rings	N	5
Coil angle	ϕ	$\frac{\pi}{4}$
crosslinked ring density	ρ	$0.05 b'^{-2}$
Physical parameters	Symbol	Values
Number of Kuhn segments in chain	$ n_t $	100
Mobile rings per subchain	p	8
Initial Kuhn length*	b'	1
Initial ring length*	c'	0.75
Component rupture stretch	λ_c	1.01
Kuhn segment stiffness*	E	1
Crosslinked ring stiffness*	E^x	1

TABLE I: Reference parameter values (assumed in-use unless stated otherwise) used to study the damage mechanics of a slide-ring unit. *Note, lengths are normalized by the length of an undeformed Kuhn segment (approximately 22 angstroms [43]) and stiffnesses are normalized by the stiffness of a carbon-carbon bond (approximately $2300k_bT$ [19]).

A. Transient behavior of a slide-ring unit

We begin by discussing the behavior of the slide-ring unit whose deformation history $\chi(t)$ is defined by Eq. (13). Once again, the loading rate plays an important role as segments rearrange within the unit to equilibrate tension. Rheological studies of slide ring gels have determined relaxation times on the order of 100 ms [47]. Furthermore, low inclusion slide ring gels display extensibility of up to 1600 % strain [48]. We here consider a wide range of loading rates parameterized by the Weissenberg number W, which may be interpreted as the loading rate $\dot{\lambda}$ normalized by the relaxation time of the material. For this study, we load each unit until one of the components has failed, which indicates the onset of damage.

To better understand the behavior of the system, we may define both unit-level quantities, which are a function of their orientation θ , as well as 'smoothed' quantities, which are averaged over all orientations. These may reflect the behavior of an ideal slide-ring network undergoing affine deformation. To begin, we define the virial stress [49] of a unit as

$$\boldsymbol{\sigma}(\theta) = \frac{1}{LH} \left[\sum_{0 \le i \le N} \boldsymbol{r}_i \otimes \boldsymbol{t}_i + \sum_{1 \le i \le N} E^x(c_i - c') \boldsymbol{c}_i \otimes \boldsymbol{u}_i \right],$$
(14)

where \otimes denotes the dyadic (tensor) product. The left part of this expression reflects the tension held within each subchain while the right expression accounts for the enthalpic force in the crosslinked rings. Note that the

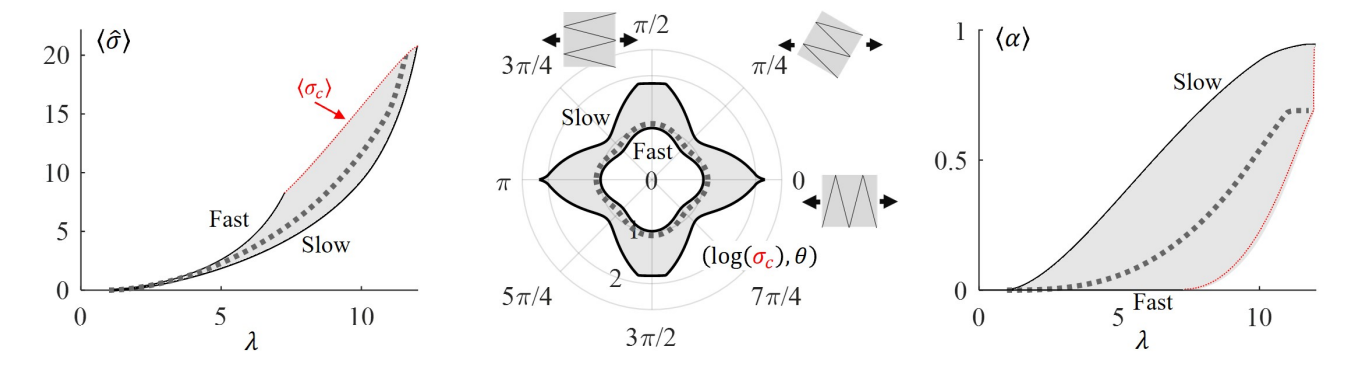


FIG. 6: Mechanical response of arbitrarily oriented units. (Left) Average principal stress on the assembly versus stretch. (Right) Average segment growth versus stretch. (Center) Critical stress versus orientation plotted on a logarithmic scale. All plots illustrate fast $(W \to \infty)$ and slow $(W \to 0)$ loading as limiting cases. The intermediate loading rate of W = 1 is illustrated with a grey dashed line.

enthalpic contribution of the Kuhn segments is already accounted for in the chain tension t. As we are deforming units with arbitrary orientation, we may consider the first principal stress $\hat{\sigma}(\theta)$ as reflecting the applied stress required to deform a unit whose edges are aligned in the direction θ . Note that the direction of $\hat{\sigma}$ may not align with θ due to the anisotropy of the unit. Furthermore, we may define the critical stress $\sigma_c(\theta)$ as the stress at which the unit fails. The other unit-level quantity of interest is the degree of sliding that has occurred during the deformation history. A simple measure of this is the fractional segment growth, denoted α , which is a normalized quantity that describes the influx of segments into the center subchains [26]. We formally define it here as

$$\alpha(\theta) = \frac{\bar{n} - \bar{n}'}{n_{\infty} - \bar{n}'},\tag{15}$$

where \bar{n} is the sum of Kuhn segments in the middle subchains and \bar{n}' is its value before deformation. With this definition, α vanishes at equilibrium and asymptotes to $\alpha = 1$ once the middle subchains have accumulated n_{∞} segments (i.e. the dangling ends have been depleted). Thus, an increase in α means segments have moved from the dangling ends into the middle subchains, while a decrease in α means that segment flux into the dangling ends has been preferred. The latter case may occur with the application of a volume-shrinking deformation, for instance. Finally, to observe the collective response of an ideal network, we may consider the network average of the quantities in Eqs. (14) and (15). For this, we define the operator $\langle \cdot \rangle$ to denote the average over all orientations θ . Fig. 6 plots the average principal stress $\langle \hat{\sigma} \rangle$, the average segment growth $\langle \alpha \rangle$, and the critical stretch $\sigma_c(\theta)$ for units deformed in all directions $0 \le \theta \le 2\pi$ to the point of rupture at varying loading rates.

Fast loading. Once again, we begin by analyzing the case of fast loading (i.e. $W \to \infty$) as it is the simplest to conceptualize. When loading a slide-ring network quickly, there is not sufficient time for sliding, and the response is that of an elastic network. This is illustrated

by the invariance of α with λ in Fig. 6. As with the aligned chain, the chain stiffens at the earliest point and subsequently fails at the smallest strain. Note that we have assumed the failure of any smoothed quantity to be governed by the weakest unit – the orientation that fails earliest dictates the critical stretch of the ensemble. Looking at the response of each unit as a function of orientation, we observe that the critical failure stress is roughly the same for all angles. Thus, the orientation of the unit does not play a large role in its mechanics at high loading rates, as would be expected for an (isotropic) elastic network.

Slow loading. In the limit of slow loading $(W \to 0)$, we expect a large transfer of segments from the dangling ends into the middle subchains (as before in the aligned case). Indeed, we notice an immediate increase in the mean fractional segment growth $\langle \alpha \rangle$, which converges to its maxmimum value of one before breaking. We also predict an increase in critical stress, critical stretch, and toughness over all orientations (Fig.6). Thus, the sliding of segments from the dangling ends increases resistance to failure as in the previous section. This time, there is a large effect of the orientation of the unit on the critical stress σ_c . In particular, units aligned orthogonal to the principal directions of loading illustrate nearly an order of magnitude increase of σ_c from the fast loading case. Units unaligned with the direction of loading experience a smaller increase in σ_c , with the smallest difference being observed at $\theta = \pi/4$ and its symmetric orientations. This is discussed further in the next section, but is ultimately due to the redistribution of segments within the middle subchains. Nonetheless, the increased critical stress is observed over all angles due to sliding and the subsequent delay of damage initiation. Thus, we may expect that networks with arbitrary topology would still have improved toughness at slow loading rates, as is observed experimentally [5].

B. Damage mechanisms of a slide-ring unit

We may now begin to consider different damage mechanisms that may occur in a slide-ring network. Recall, in this study, we consider two different possibilities for damage: rupture of crosslinked rings or rupture of Kuhn segments within a subchain. For the aligned chain, the distinction between these modes of damage was completely dictated by their relative stiffnesses (Fig. 4). For a real network, however, local geometry, loading rate, and component strength may play a role. For now, we maintain the parameters outline in Table I. This will be loosened with a parametric study in the following section.

We illustrate the damage behavior of this unit in Fig. 7. In the center, we plot the critical macroscopic stretch λ_{crit} at which a unit with orientation θ breaks for both fast and slow loading. We color the lines in this plot by their damage mechanism (which component broke first) - red for rings and blue for Kuhn segments. Once again, we note that fast and slow loading represent boundaries of the system's response. This time, we may also color the intermediate loading rate regions with the color corresponding to their preferred damage mechanism. Clearly, for this system, breaking Kuhn segments is largely preferred over a majority of orientations. We also note the slight asymmetry between angles 0 and π and angles $\pi/2$ and $3\pi/2$, which is due to higher forces being placed on either the 'middle' rings or the 'outer' rings, and subsequent preferred damage, as illustrated in the schematics. In Fig. 7, the left and right subplots illustrate the change in fractional segment growth α during loading for units aligned in the direction of loading (A: $\theta = 0$), perpendicular to the direction of loading (B: $\theta = \pi/2$), and offset to loading at $\pi/4$ rad. (C: $\theta = \pi/4$). Note that the shaded grey regions are bordered on the right by the critical stretch λ_c and segment change α that occurs at intermediate loading regimes.

Fast loading. As usual, we first consider the case of fast loading. Here, the effect of geometry is clearly observed by the 'diamond' shape outlined in the polar plot of Fig. 7. As this is the elastic regime, the reason for this is the affine deformation of the two inner-most subchains, which consistently break after a critical stretch in their respective orientation is reached. When the orientation of the unit θ is exactly aligned with the coil angle ϕ , i.e. at orientation C, we observe the smallest critical stretch as the local stretch on one of the inner-most subchains is exactly equal to the macroscopic stretch. In contrast, at orientations A and B, we observe the largest critical stretch as the relative alignment of each subchain with respect to the loading direction is equal. Interestingly, we only predict ring failure at orientations near A and B. When the middle subchains are evenly stretched, the rings sustain the highest loads, making them more vulnerable to breaking. As this regime is dominated by elastic deformation, we observe no change in α for any orientation, yielding a constant value of $\alpha = 0$ up to the border of the grey region in the plots. At this point, the

unit breaks without any sliding having occurred.

Slow loading. In the slow loading regime, we again notice an increased critical stretch over all orientations due to the influence of segment sliding. Interestingly, in this case, we observe the highest critical stretch at orientation C, while the lowest occurs at orientations A and B. Recall, when the unit is aligned normal to the deformation, all subchains are stretched uniformly. Thus, the segments that flow from the dangling ends must be evenly distributed to each subchain. This drains the dangling ends faster, as observed by the slope of the α versus λ plots, which results in a smaller critical stretch. In contrast, for the offset orientations such as C, while some inner subchains are extended, the others are compressed. This allows the compressed subchains, as well as the dangling ends, to distribute their segments into the more extended subchains. Thus, the segments in the dangling ends are depleted more slowly, and the unit is able to withstand further extension. Note that each orientation converges to its maximum value of $\alpha = 1$ before breaking, where A and B approach this value faster than C.

C. Parametric study

We may now consider the effect of the chosen parameters on the response of the unit. As shown in Table I, there are seven physical parameters that govern the mechanical properties of the chain. We first note that the initial length of Kuhn segments and mobile rings (b' and c', respectively) do not affect the stress response or damage behavior as we are considering linear spring behavior. Furthermore, the number n_t of Kuhn segments in a chain primarily dictates the point at which the chain stiffens, i.e. the applied stretch at which chains approach their contour length. Thus, the primary parameters governing the response of the unit are the strength of the components, E and E^x , and the number of mobile rings per subchain, p.

Effect of component stiffness. As demonstrated with the aligned chain, the component stiffnesses E and E^x largely influence the mode of damage preferred to the slide-ring network. For non-aligned geometries, however, local strains and non-affine deformations within the chain create a large orientation-dependence as well. To study the effect of varying the component stiffness, we consider a numerical experiment in which we strengthen only one of the components by a factor of five. Note that we are neglecting the regime of $E, E^x < 1$ for the slide-ring unit as it is unlikely to be physical (as discussed previously for the aligned chain). Fig. 8 presents the critical stretch versus orientation plots for units with strong rings (i.e. $E^x = 5$) and strong chains (i.e. E = 5). For the first case, we see that damage to the Kuhn segments has been exclusively preferred. As before, the fast loading case is driven by the geometry of the unit, while the slow loading case delays damage. In contrast, when we strengthen the

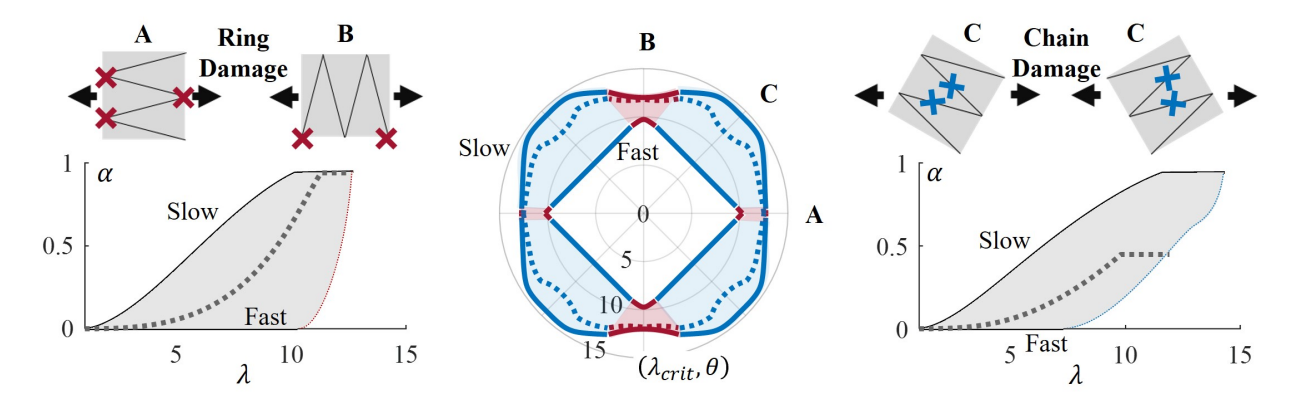


FIG. 7: Damage behavior of the unit studied in this section. (center) polar plot of the critical applied deformation at which a component breaks in a given orientation for fast, slow, and intermediate loading (W = 1, dashed). Shaded regions are colored by their preferred damage mechanism at a given orientation and loading rate (red for rings, blue for Kuhn segments). (left) Segment change versus applied stretch at orientations A and B. (right) Segment change versus applied stretch at orientation C. On both plots, the dashed curve is the response of W = 1. Note that the shaded region is bordered on the right by its predicted critical stretch at other intermediate loading rates.

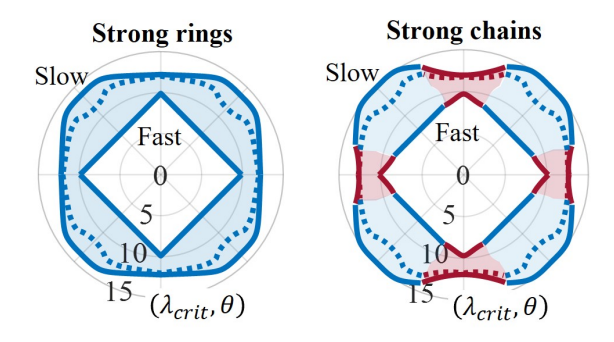


FIG. 8: The effect of component stiffness on damage behavior at fast, slow, and intermediate loading. (left) Critical stretch versus orientation for a unit with $E^x = 5$ and E = 1. Damage to Kuhn segments is exclusively preferred. (right) Critical stretch versus orientation for a unit with E = 5 and $E^x = 1$. Damage to rings is preferred at $\approx 40\%$ of orientations.

chains by a factor of five, damage to the rings is only preferred in roughly 40% of orientations. Nonetheless, there is a slight increase in the critical stretch over all orientations from the previous case due to the increased chain strength. Notice that in orientations that ring failure is preferred, which is once again centered around units oriented normal to deformation, the critical trend of λ_{crit} vs θ remains continuous. Thus, ring damage may be thought of as a limiting case in which rings fail just before the chain. Interestingly, for fast loading, the first component to fail is the chains, while for slow loading, the first component to fail is the rings.

Effect of mobile rings. The mobile rings that remain uncrosslinked after creating a slide-ring gel are known to largely influence the viscoelastic properties and fracture behavior of the material [5, 23]. In general, having too

many mobile rings hinders segment sliding due to a larger residual osmotic force. In contrast, networks with low inclusion ratios tend to have better viscoelastic properties and fracture resistance. Fig. 9 illustrates the damage behavior of units with only one mobile ring per chain up to the limit of having the same number of mobile rings as Kuhn segments in a subchain (denoted as p_{max}) for slow loading and intermediate loading (W = 1). Interestingly, we observe very similar trends from varying the number of mobile rings as we did from varying the loading rate. Indeed, increasing the loading rate and increasing the number of mobile rings both effectively prevent chain sliding from occurring during deformation. Thus, the curves illustrated for $p = p_{max}$ are, in fact, exactly the same as the curves for the fast loading rate (independent of p). This time, we notice a large increase (nearly double) of the critical stretch for units with sparse mobile rings (p=1) and units with completely full mobile rings. This fits well with the experimentally observed effect of varying the inclusion ratio [5] and further supports the claim that mobile rings at low inclusion ratios increase network toughness. Once again, it is interesting to note that while chain damage is preferred over a majority of orientations, ring damage occurs first (i.e. at a smaller λ_{crit}) in the case of slow loading.

D. Discussion

To summarize our results from the previous section, it is important to recall that fracture or failure of a material is determined by its weakest component. In this case, we may consider the orientation θ at which the critical stretch λ_{crit} is the smallest. In general, as supported by experimental evidence [5], we find that units with higher degrees of sliding are able to sustain more deformation and display higher toughness, which, in this context, may

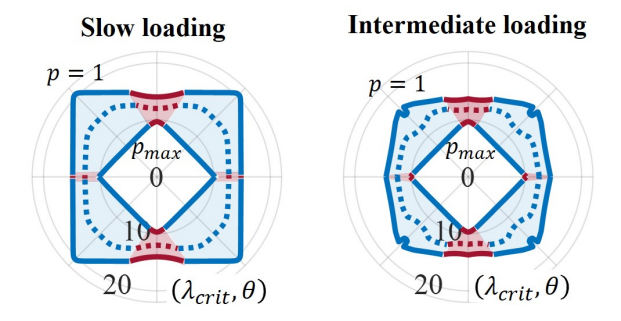
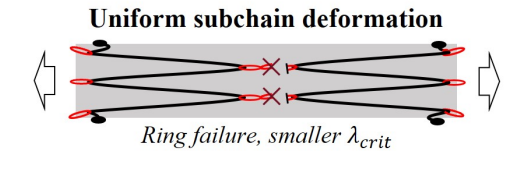


FIG. 9: The effect of mobile rings on damage behavior for a unit with mobile rings ranging from p=1 to p=n' (denoted p_{max}). (left) Deformation at the slow loading limit $(W \to 0)$. (right) Deformation at an intermediate loading rate (W=1). In both cases, $p=p_{max}$ converges to the fast loading limit as sliding is not possible. The dashed line indicates the case of p=8 for reference.

be interpreted as the amount of energy that can be supplied to a unit before failure of one of its components. The two primary factors governing the ability of a slidering network to slide efficiently are the loading rate and the inclusion ratio, which is reflected by the number p of mobile rings per subchain in our model. To obtain the toughest material, one should aim to make these two quantities as small as possible.



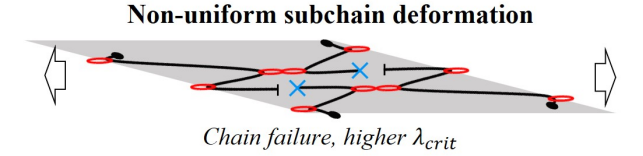


FIG. 10: Schematic: damage modes of a slide-ring unit undergoing slow loading.

One aim of this study was to add a new perspective on the potential parameters that may be adjusted to increase the performance of slide-ring materials. The effect of inclusion ratio and chain length on fracture properties are already well-known [5], but the effect of toughening network components is still unexplored. For each set of parameters studied in this paper, we find that Kuhn segments within the polymer chain are more susceptible to damage over a majority of orientations. Notably, we have observed that this is still the case even after strengthening the Kuhn segments by a factor of five (Fig. 8). This suggests that Kuhn segments are more susceptible

to damage over more orientations, but does not necessarily mean that failure in slide-ring networks is always driven by damage to the polymer chain. Clearly, increasing the strength of any component should positively affect the toughness of the material. The question of which component should be strengthened to best improve the network is determined by the orientation and component that fails at the smallest critical stretch.

When considering a slide-ring unit that can slide effectively during deformation (i.e., at relatively low loading rates and inclusion ratios), we find that the first component to fail is always the crosslinked rings. Thus, we predict that increasing the strength of crosslinked rings would yield a tougher material. To extend our study to a more physical network, one can consider two chains being loaded in tension (Fig. 10). These may reflect two different parts of an isotropic slide-ring network, for instance. If the affine motion of the crosslinked rings creates a uniform deformation of the underlying polymer chain (i.e., each subchain is stretched evenly), then segments from the dangling ends are shared among each subchain, increasing their strength uniformly, and concentrating more force on the crosslinked rings. In contrast, a chain that experiences non-uniform deformation, in which some subchains are compressed while others are extended, the highly aligned chains are much more susceptible to damage. In this study, these two cases are reflected by: (i) a unit being oriented orthogonal to the direction of loading, which creates uniform subchain deformation, and (ii) a unit whose orientation is offset to the direction of loading, which creates non-uniform subchain deformation.

V. CONCLUSION

This paper introduced a sliding network model to describe the elasticity, relaxation, and damage evolution in slide-ring units experiencing large deformations. The model conceptualizes an isotropic slide-ring network as a collection of simple units with random, yet uniform orientations. This allowed us to study a slide-ring network being deformed to the point of either chain or crosslinked ring failure. Using this approach, we find that damage to polymer chains is more likely over a majority of orientations, but damage to crosslinked rings are ultimately limiting the toughness of the network. Thus, improving the strength of the rings used during synthesis may increase the toughness of a slide-ring gel.

The present study shows how chain sliding enables the extreme extensibility of slide-ring gels. However, many of the other remarkable properties of slide-ring systems are thought to be the result of their dynamic network topology. For example, it is believed that the high fracture resistance of slide-ring gels is a product of local network rearrangements around a fracture tip [50]. This is largely due to non-affine motion of the sliding crosslinks, which may be the subject of a future study. In particular,

we may consider a mesoscale network whose components move according to local a force balance [32, 33]. This would naturally incorporate the pulley effect of tension redistribution, which is thought to be a predominant feature of slide ring networks [21]. Furthermore, this study only considers regimes prior to the onset of damage. A full network model would be required to investigate the propagation of damage in a slide ring material. In this context, the model can be used to validate many of the hypothesis proposed in experimental studies, thereby offering a fundamental understanding on the role of network design (topology, chemistry, etc.) on mechanical properties such as strength and toughness.

For clarity of presentation, our analysis remained simplistic and is therefore subject to several limitations. For instance, we varied the relative stiffness of the rings and Kuhn segment while assuming each component breaks under the same stretch. However, the stretch required to damage the bonds in a ring may differ from that required to break bonds in a Kuhn segment. More accurate results could, however, be obtained by estimating the stiffness

and stretch required to break the weakest bond within each component's structural backbone. Additionally, the purposed criteria for chain damage is exclusively the result of subchain tension. Consequently, a chain can only fail along its internal subchains as its dangling ends are tension free. However, a previous coarse grained molecular dynamics simulation found that slide-ring chains primarily fail in regions near their dangling ends [31]. This suggests chain failure should also be dependent on the osmotic force along each subchain.

ACKNOWLEDGMENTS

F.J.V. and C.B. gratefully acknowledge the support of the National Science Foundation under award no. 2023179. The content is solely the responsibility of the authors and does not necessarily represent the official views of the University of Colorado Boulder or the National Science Foundation.

- Q. Chai, Y. Jiao, and X. Yu, Hydrogels for biomedical applications: their characteristics and the mechanisms behind them, Gels 3, 6 (2017).
- [2] M. M. Perera and N. Ayres, Dynamic covalent bonds in self-healing, shape memory, and controllable stiffness hydrogels, Polymer Chemistry 11, 1410 (2020).
- [3] D. L. Taylor and M. in het Panhuis, Self-healing hydrogels, Advanced Materials 28, 9060 (2016).
- [4] F. J. Vernerey, S. Lalitha Sridhar, A. Muralidharan, and S. J. Bryant, Mechanics of 3D Cell-Hydrogel Interactions: Experiments, Models, and Mechanisms, Chemical Reviews 121, 11085 (2021), publisher: American Chemical Society.
- [5] K. Mayumi, C. Liu, Y. Yasuda, and K. Ito, Softness, elasticity, and toughness of polymer networks with slidering cross-links, Gels 7, 91 (2021).
- [6] R. Long and C. Hui, Fracture toughness of hydrogels: measurement and interpretation, Soft Matter 12, 8069 (2016).
- [7] J. P. Gong, Y. Katsuyama, T. Kurokawa, and Y. Osada, Double-network hydrogels with extremely high mechanical strength, Advanced Materials 15, 1155 (2003).
- [8] M. A. Haque, T. Kurokawa, and J. P. Gong, Super tough double network hydrogels and their application as biomaterials, Polymer 53, 1805 (2012).
- [9] K. Haraguchi and T. Takehisa, Nanocomposite hydrogels: A unique organic-inorganic network structure with extraordinary mechanical, optical, and swelling/deswelling properties, Advanced Materials 14, 1120 (2002).
- [10] K. Haraguchi, Nanocomposite hydrogels, Current Opinion in Solid State and Materials Science 11, 47 (2007).
- [11] Y. Okumura and K. Ito, The polyrotaxane gel: A topological gel by figure-of-eight cross-links, Advanced materials 13, 485 (2001).
- [12] L. Jiang, C. Liu, K. Mayumi, K. Kato, H. Yokoyama, and K. Ito, Highly stretchable and instantly recoverable slide-

- ring gels consisting of enzymatically synthesized polyrotaxane with low host coverage, Chemistry of Materials **30**, 5013 (2018).
- [13] K. Ito, Novel entropic elasticity of polymeric materials: why is slide-ring gel so soft?, Polymer Journal 44, 38 (2012).
- [14] C. Liu, H. Kadono, K. Mayumi, K. Kato, H. Yokoyama, and K. Ito, Unusual fracture behavior of slide-ring gels with movable cross-links, ACS Macro Letters 6, 1409 (2017).
- [15] A. Bin Imran, K. Esaki, H. Gotoh, T. Seki, K. Ito, Y. Sakai, and Y. Takeoka, Extremely stretchable thermosensitive hydrogels by introducing slide-ring polyrotaxane cross-linkers and ionic groups into the polymer network, Nature Communications 5, 1 (2014).
- [16] M. Doi, Soft Matter Physics (Oxford University Press, 2013).
- [17] M. Shibayama, Spatial inhomogeneity and dynamic fluctuations of polymer gels, Macromolecular Chemistry and Physics 199, 1 (1998).
- [18] M. Shibayama, Structure-mechanical property relationship of tough hydrogels, Soft Matter 8, 8030 (2012).
- [19] Y. Mao, B. Talamini, and L. Anand, Rupture of polymers by chain scission, Extreme Mechanics Letters 13, 17 (2017).
- [20] K. Ito, Novel cross-linking concept of polymer network: synthesis, structure, and properties of slide-ring gels with freely movable junctions, Polymer Journal 39, 489 (2007).
- [21] K. Ito, Slide-ring materials using topological supramolecular architecture, Current Opinion in Solid State and Materials Science 14, 28 (2010).
- [22] M. C. Boyce and E. M. Arruda, Constitutive models of rubber elasticity: a review, Rubber Chemistry and Technology 73, 504 (2000).
- [23] K. Mayumi, M. Tezuka, A. Bando, and K. Ito, Mechanics

- of slide-ring gels: novel entropic elasticity of a topological network formed by ring and string, Soft Matter 8, 8179 (2012).
- [24] M. B. Pinson, E. M. Sevick, and D. R. M. Williams, Mobile Rings on a Polyrotaxane Lead to a Yield Force, Macromolecules 46, 4191 (2013).
- [25] K. Kato, T. Yasuda, and K. Ito, Peculiar elasticity and strain hardening attributable to counteracting entropy of chain and ring in slide-ring gels, Polymer **55**, 2614 (2014).
- [26] F. J. Vernerey and S. Lamont, Transient mechanics of slide-ring networks: A continuum model, Journal of the Mechanics and Physics of Solids 146, 104212 (2021).
- [27] S. Lamont and F. J. Vernerey, A Transient Microsphere Model for Nonlinear Viscoelasticity in Dynamic Polymer Networks, Journal of Applied Mechanics 89, 10.1115/1.4052375 (2021).
- [28] S. C. Lamont, J. Mulderrig, N. Bouklas, and F. J. Vernerey, Rate-Dependent Damage Mechanics of Polymer Networks with Reversible Bonds, Macromolecules 10.1021/acs.macromol.1c01943 (2021), publisher: American Chemical Society.
- [29] Z. Zhang, G. Hou, J. Shen, J. Liu, Y. Gao, X. Zhao, and L. Zhang, Designing the slide-ring polymer network with both good mechanical and damping properties via molecular dynamics simulation, Polymers 10, 964 (2018).
- [30] Y. Yasuda, T. Masumoto, K. Mayumi, M. Toda, H. Yokoyama, H. Morita, and K. Ito, Molecular dynamics simulation and theoretical model of elasticity in slide-ring gels, ACS Macro Letters 9, 1280 (2020).
- [31] S. Uehara, Y. Wang, Y. Ootani, N. Ozawa, and M. Kubo, Molecular-level elucidation of a fracture process in slidering gels via coarse-grained molecular dynamics simulations, Macromolecules 55, 1946 (2022).
- [32] R. J. Wagner, E. Hobbs, and F. J. Vernerey, A network model of transient polymers: exploring the micromechanics of nonlinear viscoelasticity, Soft Matter 17, 8742 (2021).
- [33] R. J. Wagner, J. Dai, X. Su, and F. J. Vernerey, A mesoscale model for the micromechanical study of gels, Journal of the Mechanics and Physics of Solids 167, 104982 (2022).
- [34] Y. Masubuchi, J. Takimoto, K. Koyama, G. Ianniruberto, G. Marrucci, and F. Greco, Brownian simulations of a network of reptating primitive chains, The Journal of Chemical Physics 115, 4387 (2001).
- [35] K. Dikshit and C. J. Bruns, Post-synthesis modification of slide-ring gels for thermal and mechanical reconfiguration, Soft Matter 17, 5248 (2021), publisher: The Royal Society of Chemistry.
- [36] K. V. Dikshit, A. M. Visal, F. Janssen, A. Larsen, and C. J. Bruns, Pressure-Sensitive Supramolecular Adhesives Based on Lipoic Acid and Biofriendly Dynamic Cyclodextrin and Polyrotaxane Cross-Linkers, ACS Applied Materials & Interfaces 10.1021/acsami.3c00927 (2023),

- publisher: American Chemical Society.
- [37] Y. Mao and L. Anand, Fracture of elastomeric materials by crosslink failure, Journal of Applied Mechanics 85 (2018).
- [38] M. B. Pinson, E. M. Sevick, and D. R. Williams, Mobile rings on a polyrotaxane lead to a yield force, Macromolecules 46, 4191 (2013).
- [39] A. De Moivre, Miscellanea analytica de seriebus et quadraturis: accessere variæ considerationes de methodis comparationum, combinationum & differentiarum, solutiones difficiliorum aliquot problematum ad sortem spectantium, itemque constructiones faciles orbium planetarum, una cum determinatione maximarum & minimarum mutationum quæ in motibus corporum coelestium occurrunt (Excudebant J. Tonson & J. Watts, 1730).
- [40] W. Kuhn and F. Grün, Beziehungen zwischen elastischen konstanten und dehnungsdoppelbrechung hochelastischer stoffe, Kolloid-Zeitschrift 101, 248 (1942).
- [41] A. Cohen, A padé approximant to the inverse langevin function, Rheologica Acta **30**, 270 (1991).
- [42] A. Wineman, On the mechanics of elastomers undergoing scission and cross-linking, International Journal of Advances in Engineering Sciences and Applied Mathematics 1, 123 (2009).
- [43] K. Mayumi and K. Ito, Structure and dynamics of polyrotaxane and slide-ring materials, Polymer 51, 959 (2010).
- [44] K. Kato, K. Karube, N. Nakamura, and K. Ito, The effect of ring size on the mechanical relaxation dynamics of polyrotaxane gels, Polymer Chemistry 6, 2241 (2015).
- [45] K. Kato, Y. Ikeda, and K. Ito, Direct determination of cross-link density and its correlation with the elastic modulus of a gel with slidable cross-links, ACS Macro Letters 8, 700 (2019).
- [46] G. Wenz, B. H. Han, and A. Müller, Cyclodextrin rotaxanes and polyrotaxanes, Chemical Reviews 106, 782 (2006).
- [47] K. Kato, T. Yasuda, and K. Ito, Viscoelastic Properties of Slide-Ring Gels Reflecting Sliding Dynamics of Partial Chains and Entropy of Ring Components, Macromolecules 46, 310 (2013).
- [48] L. Jiang, C. Liu, K. Mayumi, K. Kato, H. Yokoyama, and K. Ito, Highly Stretchable and Instantly Recoverable Slide-Ring Gels Consisting of Enzymatically Synthesized Polyrotaxane with Low Host Coverage, Chemistry of Materials 30, 5013 (2018), publisher: American Chemical Society.
- [49] D. Tsai, The virial theorem and stress calculation in molecular dynamics, The Journal of Chemical Physics 70, 1375 (1979).
- [50] C. Liu, H. Kadono, H. Yokoyama, K. Mayumi, and K. Ito, Crack propagation resistance of slide-ring gels, Polymer 181, 121782 (2019).